CHEMICAL REVIEWS

Volume 96, Number 3 May 1996

Resonance Raman Intensities and Charge-Transfer Reorganization Energies

Anne B. Myers

Department of Chemistry and Center for Photoinduced Charge Transfer, University of Rochester, Rochester, New York 14627-0216

Received November 3, 1995 (Revised Manuscript Received January 29, 1996)

Contents

Anne B. Myers was born May 9, 1958, in New Haven, CT, but moved with her family to Riverside, CA, in 1961. She earned her B.S. in chemistry from the University of California, Riverside, in 1980 and her Ph.D. in biophysical chemistry from Berkeley in 1984, working with Rich Mathies. After a two-year NIH postdoctoral fellowship with Robin Hochstrasser at the University of Pennsylvania, she joined the chemistry faculty at the University of Rochester in 1987. She was promoted to Associate Professor in 1990 and to Professor in 1995. In 1995 she also became Director of the Center for Photoinduced Charge Transfer, an NSF-funded Science and Technology Center involving the University of Rochester, Eastman Kodak, and Xerox. Her research interests lie in time– and frequency–domain spectroscopic probes of fast photochemical reactions, the theory and practice of resonance Raman spectroscopy, electron transfer, and single molecule spectroscopy. She has received a Packard Fellowship in Science and Engineering, an NSF Presidential Young Investigator Award, and a Dreyfus Teacher–Scholar award, and is the author of more than 70 publications. She also enjoys distance running and qualified for the U.S. Olympic Trials in the marathon in 1992.

I. Introduction

When a molecular system undergoes a charge-transfer reaction, the equilibrium positions of the nuclei of both the reacting molecule(s) and the molecules in the environment generally change. Thus, if the reaction occurs at the equilibrium geometry of the reactant(s), the nuclei have to move in order to reach the equilibrium geometry of the product(s). The difference in energy between these two structures is referred to as the "reorganization energy", which can be decomposed into its contributions from the reacting molecule(s) ("internal" reorganization) and from the environment ("solvent" reorganization). The internal reorganization energy can be further partitioned into its contributions from individual vibrations, usually referred to as "mode-specific" reorganization energies.

Theoretical descriptions of electron transfer in the weak coupling (nonadiabatic) limit generally express the reaction rate as a product of an electronic matrix element, which depends on the distance and relative orientation of donor and acceptor, and a nuclear part, which depends on the frequencies and reorganization energies of the modes coupled to the transition.[1–4] These reorganization energies have traditionally been considered very difficult to obtain either experimentally or theoretically. However, in cases where there is also a radiative transition connecting the reactants and products, analysis of the intensities of the vibrational Raman lines obtained on resonance with the charge-transfer transition can, in principle, reveal the complete set of mode-specific reorganization energies. This article explains how and why such analyses are performed, reviews existing examples in the literature, and suggests likely future

0009-2665/96/0796-0911$25.00/0

directions for this line of research.

All electronic states have somewhat different electron distributions, so there is not always a clear distinction between charge-transfer and other electronic transitions. For the purposes of this review, a charge-transfer process is defined as one in which a full or a large fraction of an electronic charge is transferred either between two noncovalently bonded molecules or between two separate, well-defined groups within a covalently bonded structure. The former are typified by organic donor−acceptor complexes in solution, while the latter are represented predominantly by intervalence and metal-to-ligand or ligand-to-metal transitions of inorganic compounds. The literature review is limited to studies in which resonance Raman intensity data are used in at least a semiquantitative way to extract values for the geometry changes or reorganization energies accompanying a charge-transfer transition. This excludes a large number of studies in which charge-transfer resonant Raman spectra have been measured, and in some cases quantitative intensities tabulated, but the analysis needed to obtain quantitative information about excited-state geometry changes has not been performed. It also excludes many detailed and elegant resonance Raman-based analyses of geometry changes accompanying electronic excitations that are not generally considered to be of direct charge-transfer character.

II. Charge-Transfer Processes and Nuclear Reorganization Energies

Consider a process in which absorption of light formally transfers an electron from a donor moiety, D, to an acceptor moiety, A, forming an ion pair, D^+/A^-. (We will normally assume that $DA \rightarrow D^+/A^-$ is the light-driven process, but this can be generalized to the reverse situation or to cases where both the reactants and the products are charged, *e.g.* $D/A^+ \rightarrow D^+/A$.) DA and D^+/A^- represent two different electronic states whose energies depend, in general, on the coordinates of all the nuclei in the system, and these coordinate-dependent energies constitute the potential energy surfaces for the two electronic states within the Born−Oppenheimer approximation. There is no conceptual difference between these potential energy surfaces and those for any other electronic transition, but the surface for the D^+/A^- ion pair usually has a strong dependence on the solvent coordinates, particularly in polar solvents. We wish to relate the rate constant for the spontaneous, nonphotoinduced return electron transfer reaction, $D^+/A^- \rightarrow DA$, to the spectroscopic transitions, specifically resonance Raman, connecting the same two states. It should be mentioned that the ion pair can also be created by absorption to a state in which the excitation is localized on the donor or acceptor, D^* or A^*, followed by electron transfer to or from the excited donor or acceptor to form D^+/A^- whose decay is then monitored. In this case, however, the spectroscopy of the $DA \leftrightarrow D^*A$ or $DA \leftrightarrow DA^*$ transition bears no particular relationship to the kinetics of the $D^+/A^- \rightarrow DA$ process.

Since the full potential energy surfaces are functions of a very large number of nuclear coordinates, it is conventional for illustration purposes to use a reduced description in which the free energies of the neutral and ion pair states are plotted as a function of a single "reaction" coordinate, with an implied integration over the remaining nuclear degrees of freedom.[5−7] These are normally expressed as free energy plots since it is the free energy of activation, $\Delta G^‡$, that appears in the transition-state theory for the rate constant of an activated process. The reaction coordinate is usually assumed to be predominantly a solvent polarization coordinate (although this may not always be so), in which case the free energy is a quadratic function of the reaction coordinate as long as the polarization responds linearly to changes in charge distribution.[7] Two situations can now be distinguished, as depicted in Figure 1. If the two parabolas intersect such that each electronic state, at its equilibrium geometry, is the lowest energy state at that nuclear configuration as shown on the left, then the $D^+/A^- \rightarrow DA$ process is said to be in the "normal" region, while if the parabolas are nested as shown on the right, the return electron transfer is said to be in the "inverted" region. The activation energy is given by $\Delta G^‡ = [(\Delta G_0 + \lambda)^2/4\lambda]$ where ΔG_0 is the standard free energy of the reaction (negative for spontaneous reactions) and λ is the total reorganization (free) energy. The activation energy has its minimum value of zero when $\lambda = -\Delta G_0$, that is, when the two free energy curves intersect exactly at the minimum of the D^+/A^- curve.[5,8]

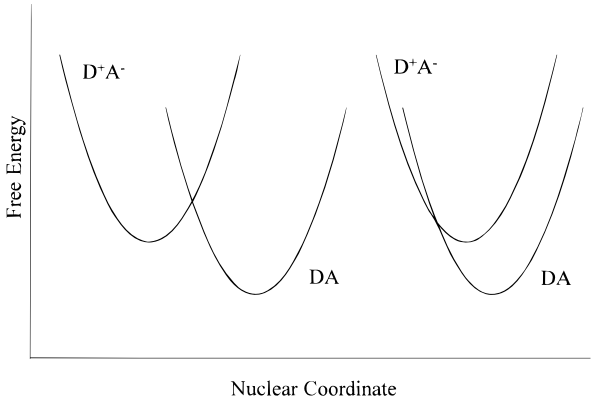

Figure 1. Relationship between free-energy surfaces for neutral and ion pair states for electron transfer in the "normal" region (left) and in the "inverted" region (right).

Nonphotochemical electron transfer in the normal region is usually treated as a classically activated process. When there is significant participation of high frequency internal modes, however, the quantum mechanical behavior of these modes must be taken into consideration.[1,9−11] Reactions deep in the inverted region are dominated by quantum mechanical tunneling and are more properly treated by radiationless transition theory.[12−16] When the coupling between the thermally populated levels of the initial state and the isoenergetic acceptor levels of the final state is small and the density of final states is large, the rate of the return electron transfer can be written as a first-order Golden Rule nonadiabatic

transition between two electronic states:

$$k = (2\pi/\hbar)|V|^2(\mathrm{FCWD}) \quad (1)$$

where V is the electronic coupling matrix element, which depends on the distance and relative orientation of electron donor and acceptor, and FCWD is the "Franck−Condon weighted density of states", which depends on the vibrational frequencies and reorganization energies for both the high-frequency internal modes and the low-frequency intermolecular and solvent coordinates. The FCWD is most often written as a sum over vibrational states each clothed in a solvent-induced line shape, but for both conceptual and computational purposes it is often more useful to cast it into an equivalent time-correlator expression,[17,18] one form of which is[19]

$$\mathrm{FCWD} = \frac{1}{\pi}\sum_w B_w \mathrm{Re}\int_0^\infty \mathrm{d}t\langle w|\exp(-i\mathrm{H}_g t/\hbar)|w\rangle \times \exp[i(\omega_{eg} + \omega_w)t - g(t)] \quad (2)$$

Here $\{|w\rangle\}$ are the multimode vibrational levels of the initial, higher energy (usually ion pair) state in the electron-transfer process, B_w is the Boltzmann population of state $|w\rangle$, $\omega_w = \epsilon_w/\hbar$ where ϵ_w is the energy above the zero-point level of this state, H_g is the vibrational Hamiltonian for the final, lower energy (usually neutral) state, ω_{eg} is the frequency separation ($\Delta E/\hbar$) between the zero-point levels of the two electronic states, and $\exp[g(t)]$ is a function, usually taken to be Gaussian, that accounts for the contribution to the total reorganization energy from low-frequency solvent and other classically behaved modes. The contribution to the total reorganization from the high-frequency quantized modes is contained in the correlation function $\langle w|\exp(-iH_g t/\hbar)|w\rangle$. Equation 2 is very closely related to the time-domain expressions from which the optical absorption and resonance Raman intensities may be calculated as described below.

Equation 2 and similar expressions that follow divide the nuclear degrees of freedom into a group of high-frequency, usually intramolecular, modes that are treated explicitly, and a group of low-frequency, usually solvent or intermolecular, modes that are treated only in a reduced, collective way as contributions to an effective line-shape function. (Note, however, there is no requirement that we do this; a generalized multimode Brownian oscillator formalism allows all nuclear degrees of freedom, with arbitrary frequencies and frictional damping, to be treated on an equal footing and incorporated into a single $g(t)$ as discussed, for example, in ref 20.) For the first group we carry out an explicit sum over the Boltzmann-weighted initial states $\{|w\rangle\}$, and the energies of these states ϵ_w are the actual eigenstate energies; when we refer to a particular mode's contribution to the reorganization energy, it may be viewed as a potential energy since the entropic contribution is zero. The line-shape function, on the other hand, represents a thermally averaged density of states weighted by their Franck−Condon factors for all the bath coordinates and thereby includes an entropic contribution, and the reorganization energy associated with this effective reduced coordinate is properly a free energy.

III. Resonance Raman Intensities

In spontaneous Raman scattering, radiation with frequency ω_L and usually linear polarization is incident on the sample, and scattered light at frequency ω_S is collected within some range of angles $\mathrm{d}\Omega$, either with or without polarization selectivity. The Raman-scattered power, $P_{scatt}(\omega_S)$, is related to the incident intensity, $I(\omega_L)$, by[21]

$$P_{scatt}(\omega_S)\,\mathrm{d}\omega_S = NI(\omega_L)\sum_i B_i \sum_f (\mathrm{d}\sigma_{if}/\mathrm{d}\Omega)L_{if}(\omega_L,\omega_S)\,\mathrm{d}\omega_S\,\mathrm{d}\Omega \quad (3)$$

Here N is the number of scatterers, B_i is the initial Boltzmann population of vibrational state $|i\rangle$, L_{if} is the normalized vibrational line shape of the $|i\rangle \rightarrow |f\rangle$ transition, and $(\mathrm{d}\sigma_{if}/\mathrm{d}\Omega)$ is the differential Raman cross section for the $|i\rangle \rightarrow |f\rangle$ transition. Integration over the finite experimental frequency bandwidth and solid angle of collection gives the detected power. The line shape of the Raman transition depends on the ground-state vibrational dynamics (although see ref 22), but the information about excited-state processes such as electron transfer is contained in the cross sections, which determine the total band-integrated intensities. Therefore it is usual to integrate eq 3 over all solid angles and over all frequencies contributing to a particular Raman line, leading to the following expression for the total scattered power arising from the $|i\rangle \rightarrow |f\rangle$ Raman transition:

$$P_{scatt}(i\rightarrow f) = NI(\omega_L)\sigma_{if}(\omega_L) \quad (4)$$

In analyzing experimental data it is often necessary to deconvolve contributions to the total intensity from overlapping transitions, and it should be kept in mind that what appears to be a single band may have contributions from multiple hot bands that originate from different initial states but involve the same quantum number changes.

The fundamental theoretical expression for the Raman cross section was originally derived by Kramers and Heisenberg in 1925[23] and by Dirac in 1927.[24] Raman scattering is a two-photon process in which the system passes from state $|i\rangle$ to state $|f\rangle$ through a set of "virtual" states $|v\rangle$ that include, in general, vibrational levels of all of the system's excited electronic states. However, when the excitation is on or near resonance with one particular electronic state, vibrational levels of that state become the dominant virtual states, and the "nonresonant" term, in which the scattered photon is formally emitted before the incident photon is absorbed, can be neglected relative to the resonant term.

A number of further simplifications and specializations of the Kramers−Heisenberg−Dirac (KHD) expression are usually assumed under conditions of electronic resonance. Most modern treatments of resonance Raman intensities follow closely or are equivalent to the development of Albrecht and coworkers in the 1960s, as summarized in ref 25. The Born−Oppenheimer approximation is employed to separate the vibronic states into products of elec-

tronic and vibrational states, and the transition dipole moments are expanded as a Taylor series in the nuclear coordinates. Collecting terms of like power in the nuclear coordinates gives for the cross section of a particular resonance Raman transition

$$\sigma_{if}(\omega_L) \propto |A_{if} + B_{if} + C_{if} + ...|^2 \qquad (5)$$

The *A* term involves only the electronic transition moment evaluated at the equilibrium internuclear geometry, while the higher terms contain the dependence of the transition moment on the vibrational coordinates. The *A* term is expected to be the most important contributor to all Raman intensities (fundamentals, overtones, and combination bands) when on resonance with a strongly allowed electronic transition. If, on the other hand, the electronic transition dipole moment is zero or small, as for resonance with a weak or forbidden electronic transition, or the scattering is to a non-totally symmetric vibrational state, then higher terms must be considered. The relationship between resonance Raman intensities and excited-state vibrational dynamics is clearest when *A*-term scattering is dominant, and Raman spectra that are dominated by totally symmetric vibrations are often interpreted assuming *A*-term activity alone. However, this assumption may be less secure for resonance with charge-transfer states than in most other electronic transitions due to the expectedly large dependence of the electronictransition moment on specific vibrations that modulate the donor−acceptor distance.

The *A*, *B*, and *C* terms in the original derivations were expressed as summations over intermediate vibrational states weighted by energy denominators. This formulation turns out to be very difficult to evaluate quantitatively for large molecules having many vibrational degrees of freedom and, also, obscures the connection between the resonance Raman intensity and the excited-state nuclear dynamics. Thus many workers have chosen to focus on the equivalent "time-dependent" formulation originally derived by Lee and Heller in 1979.[26] The *A* term is given by an expression similar to eq 2:

$$A_{if} = |\mu_{eg}|^2 \int_0^\infty dt \langle f|\exp(-iH_e t/\hbar)|i\rangle \times \exp[i(\omega_L - \omega_{eg} + \omega_i)t - g(t)] \quad (6)$$

where μ_{eg} is the electronic transition dipole moment evaluated at the equilibrium nuclear geometry and H_e is the Hamiltonian for the excited electronic state. The interpretation of this expression in terms of overlaps of moving wavepackets[26−30] is summarized in Figure 2. Interaction of the initial quantum state $|i\rangle$ with the incident radiation transfers a portion of the initial vibrational wave function to the excited-state potential surface, where it becomes a moving wavepacket propagating under the influence of the excited-state vibrational Hamiltonian, H_e. The ordinary linear absorption *band shape* depends on a Fourier transform of the overlap between this moving wavepacket, $|i(t)\rangle = \exp(-iH_e t/\hbar)|i\rangle$, and itself at time zero, $\langle i|i(t)\rangle$, while the band-integrated resonance Raman *intensity* of a particular $|i\rangle \rightarrow |f\rangle$ transition depends on the modulus squared of a half-Fourier transform of the overlap between the moving wavepacket and the final stationary state, $\langle f|i(t)\rangle$. In order for a particular $|i\rangle \rightarrow |f\rangle$ transition to have intensity, the resonant electronic state's potential energy surface must have a significantly different vibrational frequency and/or potential minimum along the normal mode(s) in which $|i\rangle$ and $|f\rangle$ differ; otherwise $|i\rangle$, which is initially orthogonal to $|f\rangle$, will remain nearly orthogonal even after propagation by H_e. In other words, those modes that are Franck−Condon active in the electronic transition are the same modes expected to show resonance Raman activity. The time-dependent formulation highlights the fact that both linear absorption and resonance Raman depend on the dynamics of nuclear motion immediately following electronic excitation. However, while the absorption spectrum depends on the dynamics along all nuclear degrees of freedom in a collective way, the resonance Raman intensity of a specific transition reflects the projection of this wavepacket motion onto one or more particular ground-state vibrational normal modes, allowing mode-specific analysis of the dynamics. Additionally, eq 2 shows that the nonradiative electron-transfer transition from the upper to the lower electronic state (as well as the charge-

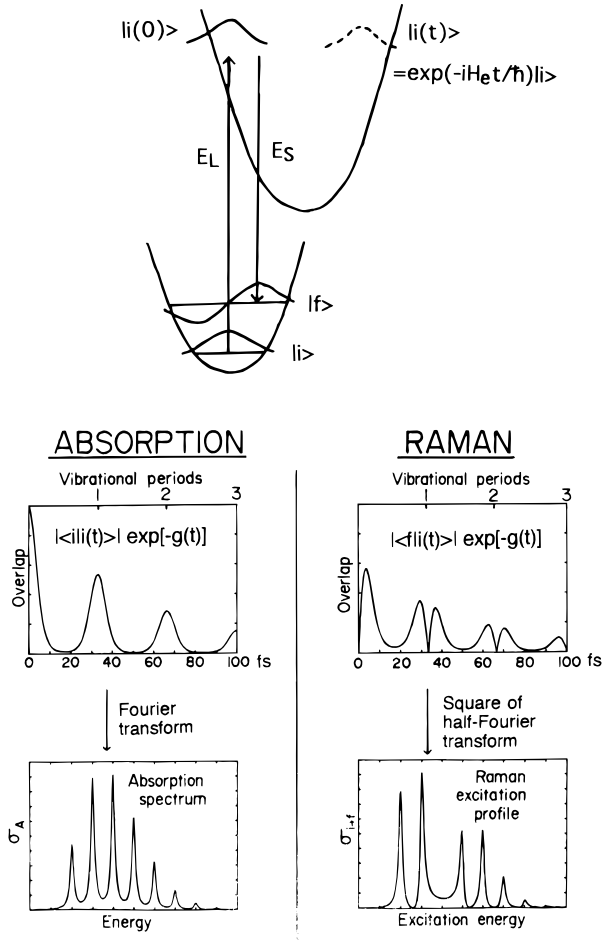

Figure 2. The time-domain view of resonance Raman scattering. The initial ground-state wave function, $|i\rangle$, is "lifted" to the excited-state surface where it becomes a moving wavepacket, $|i(t)\rangle$, propagated by the excited-state vibrational Hamiltonian, H_e. The half-Fourier transform of the overlap of this moving wavepacket with the final state in the Raman process, $|f\rangle$, gives the resonance Raman excitation profile for that mode. The full Fourier transform of the overlap of $|i(t)\rangle$ with itself at time zero, $|i\rangle$, gives the optical absorption spectrum.

recombination fluorescence connecting the same two states)[19] involves the closely related reverse problem of propagating vibrational wave functions of the upper electronic surface, $|w\rangle$, on the ground-state surface via H_g.

For displaced but undistorted oscillators (*i.e.* the ground and excited state surfaces have different equilibrium geometries but the same vibrational frequencies), the relative intensities of two Raman fundamentals in the *preresonance* region should be given approximately by[27]

$$I_1/I_2 = (\Delta_1\omega_1/\Delta_2\omega_2)^2 \tag{7}$$

where ω_j is the vibrational frequency and Δ_j is the displacement between ground and excited-state potential minima in dimensionless normal coordinates of mode j. If normal mode j is accurately described as a pure bond stretch having reduced mass μ, then the change in equilibrium bond length between ground and excited states, δr, is related to Δ by

$$\delta r = (\hbar/\mu\omega)^{1/2}\Delta \tag{8}$$

Usually, however, conversion from dimensionless to dimensioned displacements is less straightforward and requires a complete normal mode analysis of the ground-state vibrations.[29] The reorganization energy in mode j is related to the excited-state displacement and the ground- and excited-state frequencies by

$$\lambda_j = (\omega_{ej}^2/\omega_{gj})\Delta_j^2/2 \tag{9}$$

where Δ_j is expressed in dimensionless normal coordinates of the *ground* state. If the ground- and excited-state frequencies are assumed to be equal, one obtains the simpler formula

$$\lambda_j = \omega_j\Delta_j^2/2 \tag{10}$$

Equation 6 implies that the time scale of the dynamics that contribute to the resonance Raman intensity should extend for as long as the $e^{-g(t)}$ damping factor is nonnegligible. In practice, though, in most fairly large molecules the intensities are determined almost entirely by the dynamics within less than a vibrational period (typically only 10−20 fs or so). This is because the overlap $\langle f|i(t)\rangle$ involves all $3N - 6$ vibrational modes, and for this overlap to be large for a fundamental or low overtone the wavepacket must be near the Franck−Condon region along all of the other vibrational coordinates that are not excited in the transition. In a large molecule the wavepacket typically moves simultaneously along many coordinates having different frequencies, and once it leaves the Franck−Condon region it essentially never returns. Thus, *either* very rapid damping due to the $e^{-g(t)}$ factor *or* significant reorganization along multiple vibrational coordinates will lead to "short-time" behavior, meaning that the time integral need be evaluated for only a fraction of a typical vibrational period in order to accurately reproduce the spectra. In this limit, the approximate result of eq 7 is recovered without the need to assume small displacements or preresonant excitation. The quantity $\Delta^2\omega^2$ is simply the derivative of the excited-state potential surface along the vibrational coordinate at the ground-state equilibrium position,[31] and eq 7 is best interpreted to mean that when only short-time dynamics are important, the relative resonance Raman intensities are given by the relative *slopes* of the vertical excited-state surface along the various ground-state dimensionless normal coordinates.

Equation 7, and its analogs for overtones and combination bands,[27] provide an appealingly simple approximate relationship between experimental intensities and excited-state geometry changes. However, it is not clear how generally good an approximation it is. Observation of a completely unstructured absorption spectrum is often taken as evidence for short-time dynamics, but one cannot necessarily assume that the lack of structure is actually due to dynamics rather than to inhomogeneous broadening. Fundamental transitions often derive much of their intensity from preresonance enhancement from higher lying electronic states, making indiscriminate application of simple formulas dangerous.[32−34] Finally, eq 7 gives only relative displacements. One way to convert these to absolute displacements assumes that the overall breadth of the absorption spectrum is due only to the Franck−Condon activity in those modes that are high enough in frequency to be observed as distinct Raman lines. In that case, one can show that[27]

$$W = 2[\sum_k \Delta_k^2(\omega_k/2\pi)^2]^{1/2} \tag{11}$$

where W is the full width at $1/e$ height of the absorption band. However, this expression neglects contributions to the overall absorption width from solvent reorganization and electronic inhomogeneous broadening, which may often be large for charge-transfer transitions. In order to be confident that the source of the resonance enhancement is well understood, it is always best to obtain Raman data at a number of excitation wavelengths and then demonstrate, by explicit modeling of the absorption spectra and resonance Raman intensities using eq 6 and its analog for absorption,[21,29,35] that both the Raman profiles and the absorption spectrum are consistent with the same set of photophysical parameters. This generally requires a trial-and-error approach in which the excited-state potential surface and broadening parameters are iteratively refined to obtain a simultaneous best fit to the data. These modeling procedures are discussed in detail elsewhere.[21,29]

An alternative approach to evaluating resonance Raman intensity data is the "transform theory" method, originally developed by Page and coworkers[36−41] and since refined and extended by others.[42−49] The transform method exploits the close similarity between optical absorption and resonance Raman scattering to show that, under certain approximations, the band shape of the resonance Raman excitation profile can be expressed as a simple function of the Kramers−Kronig transform of the absorption spectrum. Comparison of the band shapes of the experimental and predicted profiles thus can be used to determine the validity of the assumptions made in the analysis, and the overall scaling of the profiles can provide relative, and in some cases absolute, values for the displacements. The great

attraction of transform theory is that it eliminates the need for iterative fitting, which can be quite time consuming in large molecules due to the number of parameters to be varied. However, when the simplest assumptions do not hold—*e.g.* when non-Condon effects (not pure A-term scattering) or inhomogeneous broadening are important—much of the simplicity of the transform is lost.[40,50] Furthermore, it provides no information about reorganization in modes such as solvent coordinates that are not directly observed in the resonance Raman spectrum but may be very important in charge-transfer transitions.

The question of how to handle the solvent in analyzing and modeling resonance Raman intensities is still a matter of considerable debate. One complication is that the KHD equation (in either sum-over-states or time-domain form) is not even valid, in principle, for a chromophore that is interacting with an environment unless all of the degrees of freedom of both the chromophore and the solvent are explicitly included in the modeling.[51−54] Usually this is not practical; one would like instead to treat the "uninteresting" coordinates of the environment in some kind of averaged way, which properly requires a density matrix approach. Calculation of the monochromatically excited emission for a system interacting with a bath shows that the spectrum should consist of both sharp, Rayleigh and Raman-type emission and broad, fluorescent-type emission, which are not necessarily separable either experimentally or theoretically. Usually it is simply assumed that all of the relevant time scales for solvent motion are either very slow or very fast compared with the time scale for the Raman process, which is properly determined by the ground-state vibrational dephasing (inverse homogeneous line width). In this case, the Raman and fluorescence components should be experimentally distinguishable to a good approximation, and the Raman part can still be expressed by a KHD-like equation in which the slow solvent degrees of freedom are included as inhomogeneous broadening at the Raman cross-section level while the fast solvent motions are included by replacing the simple exponential lifetime damping, $e^{-\gamma t}$, with the more general broadening function $e^{-g(t)}$ in eqs 2 and 6. The reader is referred to the original papers,[51,52] a recent review,[21] and a very clear experimental demonstration[55] for more detail.

Solvent-induced inhomogeneous broadening is nearly always treated as a Gaussian distribution of electronic zero−zero energies. There is good theoretical support for this, although inhomogeneous broadening need not always have a Gaussian form.[56] The proper functional form(s) for the "homogeneous" environmental broadening (that which appears within the Raman amplitude) is more in dispute. Early treatments simply used a very large Lorentzian line width, implying very fast exponential dephasing of the electronic coherence. Later, a number of workers utilized a stochastic model that treats the electronic line broadening as resulting from random perturbations of the transition energy by environmental fluctuations.[51,52,57−61] Depending on the rate of the fluctuations relative to their average magnitude, the resulting line shape can vary all the way from Lorentzian ("fast modulation" or "motional narrowing" limit) to almost Gaussian ("slow modulation" limit) even though the time scale is still fast relative to the ground-state vibrational dephasing. The stochastic model, while widely used, has the serious drawback for charge-transfer systems that it considers the effect of the solvent on the solute, but not *vice versa*. In particular, it does not account for solvent reorganization and the resulting solvent-induced Stokes shift of fluorescence relative to absorption. A more realistic model is the Brownian oscillator, which treats the solvent coordinates as one or more damped and displaced harmonic oscillators. In the strongly overdamped limit this model behaves very much like the stochastic model in that it can interpolate from nearly Lorentzian to nearly Gaussian broadening, but it properly incorporates the solvent Stokes shift. Again, the reader is referred to the original papers for more discussion of this model and its applications.[62−67]

IV. Applications of Resonance Raman Intensities to Charge-Transfer Processes

A. Metal-to-Ligand and Ligand-to-Metal Charge Transfer Transitions

The development of continuous-wave ion and dye lasers as practical laboratory tools in the 1970s led to a renaissance in the technique of resonance Raman spectroscopy. Transition metal complexes, with their visible absorption bands, usually weak fluorescence, and frequently high photostability, were among the most widely studied compounds. While much of the early work was qualitative, the theory of resonance Raman intensities was undergoing development at the same time, and some of the earliest studies that quantitatively analyzed intensities to determine excited-state geometries involved charge-transfer states of transition metal complexes.

Particularly notable was the study by Spiro and co-workers of metal-to-ligand charge transfer (MLCT) in a bis(pyridine)iron(II) heme.[68] These workers used the argon ion laser lines from 458 to 514 nm to measure Raman excitation profiles on resonance with a weak feature in the absorption spectrum, to the blue of the main visible Q_0 band and its vibronic sidebands, which had been tentatively assigned as a Fe(II) → pyridine charge-transfer band. In addition to numerous weak porphyrin vibrations, they observed strong Raman transitions localized on the pyridine ligand as well as the symmetric iron−pyridine stretch, and the profiles for all of these modes peaked at about the same wavelength, somewhat to the blue of the charge-transfer absorption maximum. The relative intensities at the excitation profile maximum were used to calculate dimensionless excited-state displacements through an approximate relationship that is slightly more rigorous than eq 7,[69,70] and the results of a normal mode analysis were then used to convert the dimensionless displacements to actual bond length and bond angle changes.

These workers also used relative intensities for the pyridine-d_5 isotopomer (see Figure 3) to help distinguish among the many possible geometries that are

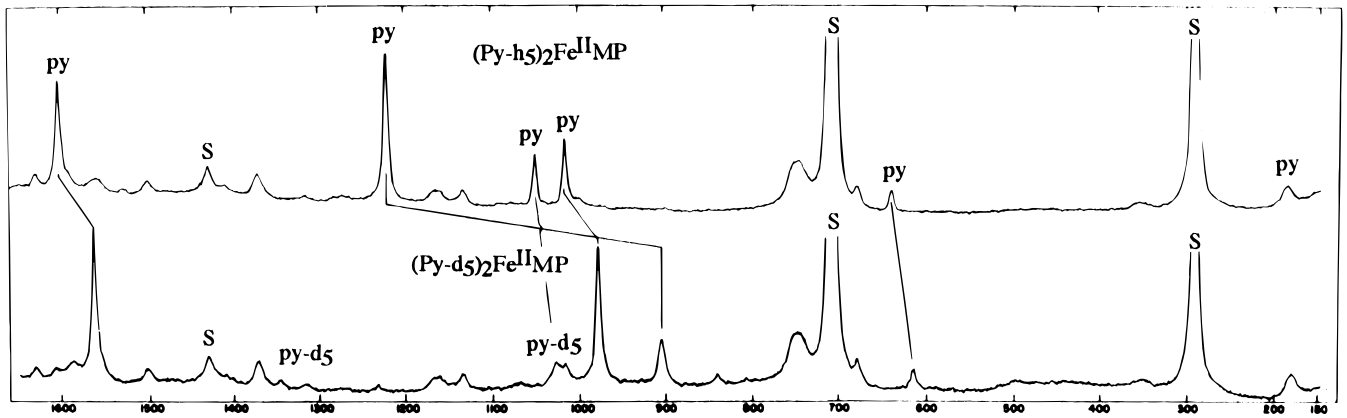

Figure 3. Resonance Raman spectra of fully protonated (top) and fully deuteriated (bottom) $(Py)_2Fe^{II}(MP)$ (MP = mesoporphyrin IX dimethyl ester) in CH_2Cl_2 with 476.5 nm excitation, on resonance with the $Fe^{II} \rightarrow$ pyridine charge-transfer transition. Transitions due to the bound pyridine (py) and the solvent (S) are labeled; other bands are due to the porphyrin ligand. (Reproduced with permission from ref 68. Copyright 1979 American Chemical Society.)

equally consistent with the experimental intensities. This ambiguity arises because the resonance Raman intensities, at *any* level of theory that assumes separable vibrational modes, depend only on the absolute magnitude of the displacements Δ, not on their signs. Therefore, if (as in this case) there are six vibrations with significant intensity, there are $2^6 = 64$ different sign combinations, and therefore 64 different excited-state geometries, which are identically consistent with the experimental intensities. The intensities of isotopic derivatives provide a means of distinguishing among these solutions, since isotopic substitution affects the normal mode compositions but presumably not the equilibrium geometries.[29,71] Thus, if one had exact ground-state normal mode descriptions and a perfect model for the resonance Raman intensities and calculated all 64 excited-state geometry changes for both isotopomers, only the one correct choice of signs should give the same geometry for both isotopomers. In practice the analysis always has some deficiencies, but Spiro and co-workers were able to eliminate half of the 64 possible geometries by simple physical intuition (expecting a contraction rather than an expansion of the middle C−C bonds of the pyridine rings), narrowed these down to three by using the isotopic intensity data, and compared with a molecular orbital calculation of the geometry to choose two of these as more likely than the third. These two solutions had nearly identical bond length changes in all of the relevant coordinates except the Fe−N stretch and conformed with the qualitative expectations for geometry changes upon metal-to-ligand charge transfer.

More accurate values for the dimensionless displacements could be obtained by explicitly modeling both the absorption spectrum and the excitation profiles, including the interference terms between the postresonant enhancement from the stronger Q band and the resonant scattering from the charge-transfer band. Also, more isotopic derivatives (*e.g.* ^{13}C-labeled or partially deuteriated pyridine) might allow both further refinement of the ground-state normal mode descriptions and even more precise discrimination among the different possible sign combinations of the normal mode displacements. Nevertheless, this work as it stands remains one of the most detailed analyses of excited-state geometry changes from resonance Raman intensities yet reported.

One of the earliest Raman intensity analyses to make use of the time-domain picture of resonance Raman scattering was the work of Yang and Zink on the MLCT (Cr→NO) transition of $K_3[Cr(CN)_5NO]$.[72] They used a simple formula, analogous to eq 7, to calculate the displacement in the dominant Cr−N stretching mode from its fundamental to overtone intensity ratio. They then used eq 7 to determine the displacements in three other modes that clearly exhibited only fundamentals and showed that these four modes alone with their Raman-determined displacements gave a reasonable representation of the lower energy region of the absorption spectrum. The resonance Raman experiment was performed at only a single excitation wavelength, 514.5 nm, which is nearly resonant with the apparent zero−zero transition. While data at more than one wavelength and/or absolute intensities would provide a useful check, the analysis appears internally consistent. Only qualitative conclusions about bond length changes can be made in the absence of a complete ground-state normal mode description.

The two studies described above were couched purely in terms of spectroscopic analysis of ground-to-excited-state geometry changes; the charge-transfer character of the transitions was peripheral to the analysis. The first workers to draw the connection between resonance Raman intensities and the mode-specific reorganization energies important in general electron transfer theory were Doorn and Hupp in 1989 on MLCT in $Ru(NH_3)_4(2,2'\text{-bipyridine})^{2+}$ [73] and on intervalence charge transfer in $(NC)_5Ru-CN-Ru(NH_3)_5^-$ described in part C below.[74] In $Ru(NH_3)_4(bpy)^{2+}$, they obtained Raman spectra in solution at 676.6 nm (essentially preresonant), 647.1 nm (on the red edge of the MLCT absorption), and 514.5 nm (in the region of overlap between the MLCT band and the next electronic absorption); the λ_{max} of the MLCT band is at 576 nm. Significant differences were found between the 514.5 nm spectrum and the red-excited ones, which they interpreted to indicate resonance enhancement from more than one electronic state at the bluer wavelength; they therefore limited their analysis to the red-excited spectra, and used the

Table 1. Reorganization Energies for Bipyridyl Modes in Three MLCT Transitions

ground-state frequency ω (cm^{-1})			reorganization energy λ (cm^{-1})		
$[Ru(NH_3)_4(bpy)^{2+}]$[a]	$[Ru(bpy)_3^{2+}]$[b]	$[Fe(bpy)_3^{2+}]$[c]	$[Ru(NH_3)_4(bpy)^{2+}]$[d]	$[Ru(bpy)_3^{2+}]$[e]	$[Fe(bpy)_3^{2+}]$[f]
1605	1608	1608	100	77	73
1548	1563	1566	100	170	160
1481	1491	1492	200	400	400
1331	1320	1322	82	200	240
1266	1276	1279	13	83	96
1250	1264		14	5	
1172	1176	1174	73	140	150
1106	1110	1068	36	14	29
1027	1043	1025	43	13	200
767	766		26	8	
667	668		520	190	
376	370		780	36	

[a] Reference 73. [b] Reference 76. [c] Reference 75. [d] Table III of ref 73. [e] Calculated from Table 3 of ref 76 using $\lambda = \Delta^2\omega/2$. [f] Calculated from the relative Δ values in Table 1 of ref 75 for the lower energy (ψ) MLCT band using $\lambda = \Delta^2\omega/2$, scaled to $\lambda = 400$ cm^{-1} for the 1492 cm^{-1} mode.

relative intensities with eq 7 to convert the relative Raman intensities for the 14 observed fundamentals to relative displacements and then to absolute displacements through eq 11. As the authors discussed, eq 11's neglect of the contribution of solvent reorganization to the total absorption width should result in overestimation of the internal reorganization energy; absolute cross sections or overtone to fundamental ratios could be used to check the absolute scaling of the displacements. Their analysis resulted in a total reorganization energy of 2283 cm^{-1} divided almost equally between metal−ligand stretching and bending modes and bipyridine-localized modes. In all, significant intensity was seen in 14 normal modes having frequencies from 1605 to 248 cm^{-1}. No intensity was observed in NH or CH stretching modes, as verified by examining the spectra in deuteriated DMSO. This is consistent with the qualitative expectation that hydrogen-stretching vibrations should not make significant contributions to the reorganization energy.

Shortly thereafter, Berger and McMillin measured relative Raman intensities for $Fe(bpy)_3^{2+}$ at two wavelengths, 532 and 355 nm, which are on resonance with two different, reasonably strong MLCT transitions that correspond to moving an electron from a metal d orbital into the two lowest π^* orbitals of the bipyridine ligand.[75] Nine fundamentals were observed, and the relative displacements in these normal modes were estimated from eq 7. They obtained relatively similar intensity patterns in the two charge-transfer states and concluded that the intensities were qualitatively in agreement with the expected nature of the electronic excitations, but called into question some aspects of the most recent ground-state normal-mode analysis.

More recently, Maruszewski and co-workers presented a resonance Raman intensity analysis of the MLCT state of the closely related compound $Ru(bpy)_3^{2+}$ and nine of its selectively deuteriated analogs.[76] They, like Doorn and Hupp, used the "short-time" approximations to extract absolute values of Δ from the relative Raman intensities and the absorption bandwidth, but they used excitation on the blue side of the absorption maximum at 457.8 nm. They argued that the nearly identical spectral patterns obtained with excitation at 457.8, 476.5, and 488.0 nm showed that only one electronic state contributes to the resonance enhancement at these wavelengths, but their spectra show considerably less relative intensity in low-frequency modes than do Doorn and Hupp's red-excited spectra of $Ru(NH_3)_4(bpy)^{2+}$, a difference that the latter authors had also observed and attributed to contributions from more than one electronic state at the bluer wavelength. The extensive set of isotopic intensities should be very helpful for solving the sign problem in converting from dimensionless to internal coordinate displacements as discussed above, but apparently the data have not been employed for this purpose.

Table 1 compares the reorganization energies obtained by the Hupp, Berger, and Kincaid groups for $Ru(NH_3)_4(bpy)^{2+}$, $Fe(bpy)_3^{2+}$, and $Ru(bpy)_3^{2+}$, respectively, for the modes assigned as predominantly bipyridyl vibrations. The $Fe(bpy)_3^{2+}$ numbers, published only as relative excited-state displacements, have been scaled to give the same reorganization energy in the strongest mode as determined for $Ru(bpy)_3^{2+}$. Apart from the abovementioned discrepancy between $Ru(NH_3)_4(bpy)^{2+}$ and $Ru(bpy)_3^{2+}$ in the low-frequency region, which was not examined in $Fe(bpy)_3^{2+}$, the agreement among the three molecules is fairly good with the exception of the ring-breathing mode near 1025 cm^{-1}, which appears to be much stronger in the iron compound than in the two ruthenium compounds.

Maruszewski *et al.* also measured phosphorescence lifetimes for each isotopomer, from which they extracted the rate of radiationless decay from the ^{3}MLCT state back to the ground state, and then utilized the set of vibrational frequencies and displacements for each isotopomer to try to calculate the isotope dependence of this rate. The authors couched their analysis in terms of traditional triplet → singlet radiationless transition theory[15,16] and treated the total rate as the product of two terms: an "electronic" term that depends on the vibronic coupling interaction induced by the promoting vibrational mode(s), and a "Franck−Condon" term that involves the acceptor vibrations and is basically the same as the FCWD in eq 2. While the measured nonradiative rates increased by about 50% between the fully deuteriated ligand and the fully protonated one, with intermediate degrees of deuteriation having inter-

mediate effects on the rate, the calculated rate considering only the effect of the acceptor vibrations increased by only 14% from d_8-bpy to h_8-bpy. The authors thus concluded that the main deuteriation effect must be on the promoter modes that couple the excited (Ψ_e) and ground (Ψ_g) states through the term $\sum_k \omega_k |\langle \Psi_g | (\partial/\partial Q_k) | \Psi_e \rangle|^2$, where the sum over k runs over all vibrational modes having the correct symmetry to couple the two states. They further assumed that they could neglect the mode dependence of the matrix element $\langle \Psi_g | (\partial/\partial Q_k) | \Psi_e \rangle$, thus leaving the promoter modes' contribution to the total rate as simply proportional to $\sum_k \omega_k$. Since the promoting modes are expected, by analogy with benzene, to be modes of B_2 symmetry for which experimental frequencies are not available for all the isotopomers, they calculated the frequencies using an empirical force field and found a very good correlation between experimental and calculated nonradiative rates by assuming that the B_2 modes ν_{34} and ν_{35} are the promoting modes. This is an interesting result, but the assumption that all normal modes of the same symmetry have either zero or equally large matrix elements coupling the two zeroth-order electronic states is questionable, and in view of the large number of possibilities for the single mode or pair of modes active in such coupling, the good agreement between calculated and experimental isotope effects may be fortuitous. However, the failure of the acceptor mode-only analysis to explain the isotope effects may be relevant to the similar results obtained for organic charge-transfer complexes, as discussed in section V.

Very recently, Loppnow and co-workers presented a detailed resonance Raman excitation profile and absolute cross-section analysis of the ligand-to-metal (Cys → Cu) charge-transfer transition of the blue copper protein plastocyanin.[77] They followed a similar procedure to that in ref 78 (see section E) to fit the absorption spectrum and absolute excitation profiles in order to extract the contributions of each individual mode to the reorganization energy, and assigned the remaining electronic pure dephasing required to fit the absolute cross sections to reorganization along low-frequency "solvent" (in this case, presumably protein) modes. In plastocyanin the excited-state lifetime is so short that it makes an important contribution to the total dephasing; the authors estimated a lifetime of 20 ± 15 fs, by measuring the total fluorescence yield, and removed this contribution from the total electronic dephasing to arrive at the low-frequency reorganization energy. Their analysis resulted in a reorganization energy of 1510 cm^{-1} in the "high-frequency" modes, mostly metal−ligand stretching vibrations, and an additional 480 cm^{-1} from the low-frequency motions not directly observable in the resonance Raman spectrum. The rather small low-frequency reorganization energy is consistent with the known hydrophobic (nonpolar) nature of the copper binding site. Comparison of the metal−ligand bond length changes obtained from the resonance Raman analysis with those obtained from X-ray crystal structures of the oxidized and reduced forms of plastocyanin do not appear to be in very good agreement. This may point to differences in the electronic states prepared through charge-transfer excitation of the copper center vs transfer of an electron into or out of the entire protein and may also reflect the lack of an accurate normal mode analysis for plastocyanin. It should be noted that in this system it would not be appropriate to estimate the total reorganization energy from the Stokes shift between absorption and fluorescence, since the fluorescence emerging on a 20 fs time scale must be highly vibrationally unrelaxed.

B. Ligand-to-Ligand Charge Transfer

Compared with metal-to-ligand and ligand-to-metal transitions, relatively few electronic absorptions of the ligand-to-ligand charge transfer (LLCT) type are known. Among the best studied such transitions are absorptions attributed to electron transfer from the dithiolate to the diimine ligand in metal diimine dithiolate complexes. Wootton and Zink reported resonance Raman and low-temperature luminescence analyses of the LLCT bands of two metal diimine dithiolate complexes.[79] In a 77 K ethanol glass, the absorption spectra peak near 550 nm and show weak vibronic structure. Room-temperature Raman spectra of either the pure solids or the solids diluted into KBr were obtained at 676.4 nm, which is far on the red edge of the absorption spectrum. Since the excitation is essentially preresonant and no overtone transitions were reported, enhancement from higher lying electronic states and/or the effects of coordinate dependence of the transition moment could be complicating factors. In each system 10 resonance Raman fundamentals were identified, corresponding to both metal−ligand stretching vibrations and modes localized on both ligands. Equations 7 and 11 were used to convert the relative intensities to absolute dimensionless displacements which were then slightly adjusted to improve the fits to the absorption spectra. The absorption spectra were calculated by using a coupled-surface model that explicitly takes into account the interaction between the ground and excited-state surfaces near their crossing point. This coupling was ignored in analyzing the Raman data, which might appear inconsistent, but further analysis showed that for these coupling strengths (about 2000 cm^{-1} as calculated from Marcus−Hush theory[80,81]) and given the location of the curve crossings, the intersurface couplings have a negligible effect on the spectroscopy anyway. Finally, the dimensionless displacements were converted to bond length changes by using a potential energy distribution from an empirical force field. Figure 4 shows the final bond length changes arrived at from the intensity analysis.

C. Intervalence (Metal-to-Metal) Charge Transfer

Metal-to-metal charge-transfer transitions in bridged metal dimers have long been, and continue to be, subjects of great interest in the electron-transfer community. One of the first charge-transfer transitions to be analyzed using time-dependent Raman theory was the transition $(NC)_5Ru^{II}-CN-Ru^{III}(NH_3)_5^- \rightarrow (NC)_5Ru^{III}-CN-Ru^{II}(NH_3)_5^-$ by Doorn and Hupp in 1989.[74] In aqueous solution, this unsymmetrical dimer exhibits a moderately strong

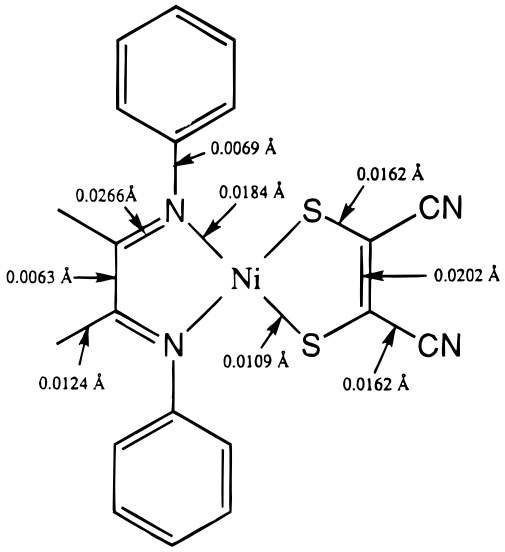

Figure 4. Absolute magnitudes of distortions in the ligand-to-ligand charge-transfer state derived from resonance Raman intensities and a ground-state normal mode analysis. (Reproduced with permission from ref 79. Copyright 1995 American Chemical Society.)

optical intervalence absorption band with $\lambda_{max} = 684$ nm. Raman spectra can be obtained near resonance, but Doorn and Hupp based their analysis on spectra excited postresonant at 514.5 nm, where the short-time limit of eq 7 is more likely to be valid. The possibility of contributions to the enhancement from higher lying electronic states was discussed, but considered not to be very important on the basis of the large energy gap between the intervalence state and the lowest locally excited states. The dominant reported Raman lines were the CN stretches, particularly the bridging CN, and six low-frequency lines between 250 and 600 cm^{-1}, assigned as metal−ligand stretching and bending modes. The intensities were converted to dimensionless displacements and then to bond-length changes under the assumption that the nominal stretches are pure local modes. These bond-length changes were shown to agree quite well with those obtained from X-ray crystal structures of related monomeric compounds. This study clearly demonstrated the participation of modes localized on both ends of the molecule in the vibrational reorganization, as well as the particularly large contribution of the bridging ligand to the total reorganization energy. These workers also examined intervalence-enhanced scattering in the closely related $Fe^{II}-Os^{III}$ bridged dimer, $(NC)_5RFe^{II}-CN-Os^{III}(NH_3)_5^- \rightarrow (NC)_5-Fe^{III}-CN-Os^{II}(NH_3)_5^-$.[82] Here the intervalence transition has a λ_{max} of 609 nm and postresonant excitation at 501 nm was used. The results were qualitatively similar to those obtained for the Ru compound, although the metal−NH_3 bending vibration, which has nearly the same frequency in both complexes, was found to have about a 4-fold larger reorganization energy in the Ru dimer than in the Fe−Os species.

In addition to the work reported on the simple bridged dimers of the type described above, intervalence transitions in linear-chain "polymeric" mixed-valence complexes have also been the subjects of a variety of resonance Raman studies, generally qualitative in nature or focused mostly on ground-state properties. One study that did attempt to extract geometry changes from excitation profiles was that of Clark and Dines on the linear-chain complex $[Pt(en)_2][Pt(en)_2Br]Br_4$ where en = 1,2-diaminoethane.[83] The visible absorption of this complex consists of a broad, strong band attributed to the dipole-allowed intervalence $Pt^{II} \rightarrow Pt^{IV}$ transition, plus a higher-energy shoulder tentatively assigned as $Br \rightarrow Pt^{IV}$ charge transfer. The resonance Raman spectra are dominated by the symmetric metal−ligand chain stretching mode, ν_1. Clark and Dines used a two electronic state, single vibrational mode model to fit the profiles for ν_1 and its first two overtones as well as the relative intensities of the first 11 members of the $n\nu_1$ progression at a single excitation wavelength and then assumed a simple local-mode picture to convert the dimensionless displacement obtained to a bond length change. The absorption spectra themselves were apparently not modeled nor were absolute cross sections obtained, and it is not clear how sensitive the Raman profiles and spectra are to the numerous parameters of the model. The final fitting parameters used the same homogeneous line width and excited-state displacement in both electronic states, while different (large) inhomogeneous widths were obtained for the two states.

More recently, Hupp and co-workers have turned their attention to intervalence transitions in symmetric mixed-valence dimers,[84−86] of which the classic example is the Creutz−Taube ion, $(NH_3)_5Ru-pyrazine-Ru(NH_3)_5^{5+}$.[87] These complexes present special experimental challenges because the intervalence transitions typically occur in the near-infrared region of the spectrum where resonance Raman measurements are notoriously difficult. An early study used 1064 nm excitation to examine the Raman spectra of three such symmetric dimers involving Ru or Fe as metals with bipyridine, NH_3, and cyano ligands.[84] While spectra of two of the complexes were obtained, comparison of the mixed-valence dimers with their oxidized and reduced congeners (which have no resonant charge-transfer transition) indicated that the intensity was arising mainly from preresonant MLCT transitions and not the intervalence transitions of interest. More recently, however, Hupp and co-workers succeeeded in obtaining intervalence-enhanced spectra of the Creutz−Taube ion itself by combining Nd:YAG laser excitation at 1320 and 1337 nm with a liquid nitrogen-cooled germanium detector (Figure 5).[85,86] The mixed-valence ion at these wavelengths exhibited significant resonance enhancement over that observed with 1064 nm excitation and over that obtained from the oxidized and reduced forms of the ion, which are nonchromophoric in the near-IR. At least eight vibrational fundamentals were observed and assigned, and their reorganization energies obtained by fitting both the Raman intensities and the absorption spectrum. While the dominant vibrations were found to be, as expected, metal−ligand stretches along the metal−bridge−metal axis, several pyrazine localized vibrations were also found to be active. These are extremely difficult experiments to carry out at present, but continuing improvements in near-infrared array detectors should improve the situation in the future.

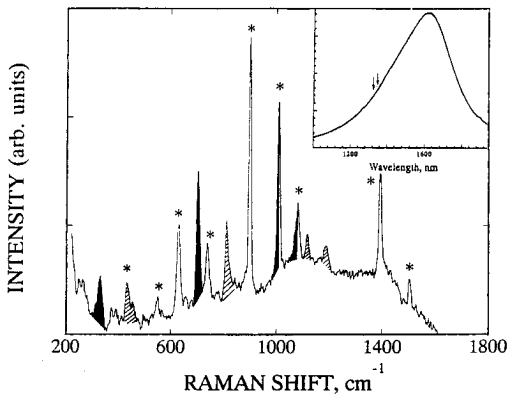

Figure 5. Resonance Raman spectrum of the Creutz–Taube ion, $(NH_3)_5Ru(pyrazine)Ru(NH_3)_5^{5+}$, with excitation at 1320 nm (peaks in black). Duplicate peaks from the excitation line at 1337 nm are cross-hatched, and asterisks indicate solvent peaks or reflections. Inset: absorption spectrum. (Reproduced with permission from ref 86. Copyright 1994 American Chemical Society.)

D. Interfacial Charge Transfer

The electron-transfer reactions of most interest to electrochemists are interfacial ones, *e.g.* between a molecule and an electrode surface. Interfacial electron transfer is amenable to resonance Raman analysis if it can be photochemically induced, and one such reaction, optical electron transfer from $Fe(CN)_6^{4-}$ to TiO_2, has been studied by the Hupp group.[82,88] Addition of potassium ferrocyanide to aqueous colloidal TiO_2 sols produced stable assemblies characterized by a strong ($\epsilon = 5000$ M^{-1} cm^{-1}), broad surface intervalence charge-transfer absorption peaked near 410 nm. Excitation at 488.0 nm, within the absorption band, revealed 10 Raman lines between 300 and 2200 cm^{-1} which were shown to be resonance enhanced by comparison with spectra excited at 514.5 and 647.1 nm and by comparison with ferrocyanide alone and colloidal TiO_2 alone. Since the charge-transfer absorption spectrum is not clearly isolated from locally excited bands and from background scattering, eq 7 was used to obtain relative displacements only, while the absolute Δ values were obtained by scaling to crystallographically determined bond length changes for the nonbridging Fe–C bonds in $Fe(CN)_6^{3-/4-}$. As for the binuclear metal complexes discussed in section C above, the greatest displacements were obtained in bridging modes, with the bridging CN stretch accounting for about 40% of the total high-frequency vibrational reorganization. In addition, three vibrations assigned as Ti–O stretches of the surface itself were significantly resonance enhanced, an interesting result that is at odds with the traditional view of interfacial electron transfer which assumes no change in the surface structure accompanying the reaction.

E. Noncovalent Donor–Acceptor Complexes

The charge-transfer absorption bands of noncovalent electron donor–acceptor complexes were among the first to be studied by laser resonance Raman techniques, but only recently were the intensities and/or excitation profiles analyzed quantitatively or the results connected with electron-transfer theory. Hupp and co-workers obtained mode-specific reorganization energies for reduction of the 4-cyano-*N*-methylpyridinium cation by forming a complex between the cation and iodide ion and exciting on resonance with its charge-transfer absorption.[89] Although the transition is fairly weak ($\epsilon << 1000$ M^{-1} cm^{-1}), it was shown to provide substantial resonance enhancement of coupled vibrations as determined through examination of the excitation profiles and depolarization ratios, and the greatly reduced scattering intensity when iodide was replaced by chloride. Under the assumption that all Raman intensity is enhanced by the charge-transfer transition and that short-time dynamics hold, eqs 7 and 11 were used to convert the observed intensities for 13 modes between 400 and 2250 cm^{-1} to excited-state displacements. Unfortunately no overtone or combination band transitions were observed which could serve as checks for the accuracy of the analysis, and the spectra did not extend to sufficiently low frequencies to permit detection of the intermolecular stretching mode, which might be expected to show considerable resonance enhancement.

The charge-transfer complex most widely studied by resonance Raman techniques is that between hexamethylbenzene as electron donor and tetracyanoethylene as acceptor. This system forms a ground-state complex with a large equilibrium constant that absorbs strongly in the middle of the visible spectrum, far from any locally excited transitions of donor or acceptor. The ground-state equilibrium constants and structures of both the 1:1 and the 2:1 (DAD) complexes, and the electronic and vibrational spectroscopy of this complex, have been studied extensively in a variety of solvents. Several vibrations of this complex were also the subject of a very early resonance Raman excitation profile study.[90] Other resonance Raman studies have focused on the low-frequency, presumed intermolecular stretching mode of this complex, and related complexes of TCNE with other donors.[91,92] More recently, two groups have used theoretical modeling of resonance Raman excitation profiles, including absolute cross sections, to obtain the charge-transfer excited-state geometry changes for the HMB/TCNE complex.[78,93–96]

Myers, Gould, and co-workers obtained absolute excitation profiles for 11 fundamentals, which included modes localized on both the donor and the acceptor as well as the low-frequency presumed intermolecular stretch mode. A number of overtones and combination bands were also observed (Figure 6). They then simulated the absorption spectrum and excitation profiles in CCl_4 with a model that explicitly included all 11 fundamentals plus an overdamped Brownian oscillator to represent the solvent. The original analysis did not include the fluorescence spectrum, and the best fit yielded a low electronic zero–zero energy and a large "solvent" reorganization energy, which seemed suspect in a nonpolar solvent.[78] Incorporation of the weak, far-red fluorescence spectrum to constrain the model resulted in a considerably higher zero–zero energy and lower total reorganization energy, but the relative weakness of the observable resonance Raman lines above 100 cm^{-1} still required a large amount of electronic spectral broadening presumably due to

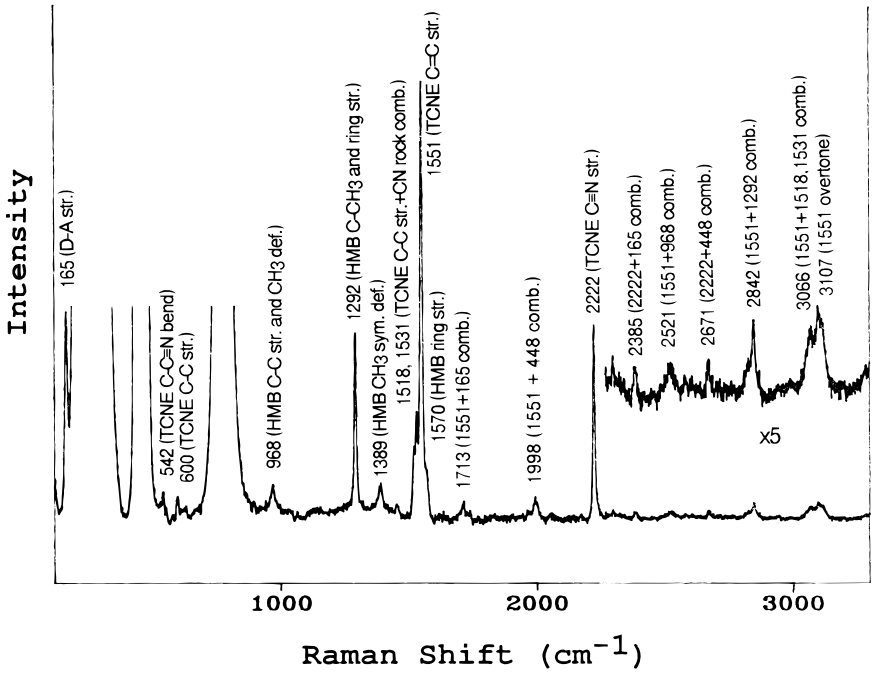

Figure 6. Resonance Raman spectrum of the hexamethylbenzene/tetracyanoethylene charge-transfer complex in CCl_4 with excitation at 514 nm. The unlabeled off-scale bands are due to solvent. All bands above 2300 cm^{-1} are combination bands or overtones. Experimental details are given in ref 78.

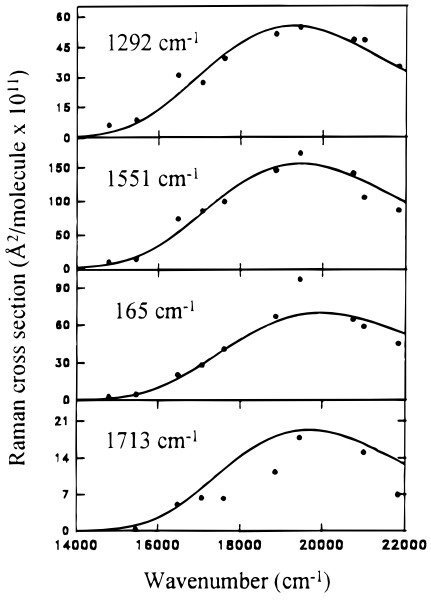

Figure 7. Calculated fits to the resonance Raman excitation profiles of hexamethylbenzene/tetracyanoethylene in CCl_4 using parameters that also reproduce the absorption and fluorescence spectra. (Reproduced with permission from ref 131.)

reorganization along unobserved, low-frequency motions (Figure 7).[94] It was suggested that much of this apparent "solvent" reorganization energy may in fact be due to the other five low-frequency intermolecular modes that are not observed in the Raman spectrum. A variety of observations, including the apparent breakdown of the Strickler−Berg relations connecting absorption strength with emission lifetime and yield,[94] suggest that the relaxed ion-pair state may be very different from the vertically excited charge-transfer state in these conformationally labile noncovalent complexes. This group also examined the resonance Raman, absorption, and fluorescence spectra of the complex formed with perdeuteriated HMB and found that the resonance Raman-active modes involve little hydrogen motion.[96] This result, however, is hard to rationalize with the substantial deuterium isotope effect on the radiationless return electron transfer, as discussed in section V below.

McHale and co-workers used CH_2Cl_2 as the solvent and measured more detailed excitation profiles, but examined only the four strongest resonance Raman lines. They originally used transform theory to analyze their profiles,[93] but later published a full paper in which these four modes of the complex and a stochastic line broadening function for the solvent were employed to explicitly model the absorption spectrum and excitation profiles.[95] Their experimental excitation profiles all peaked above 20 000 cm^{-1}, considerably blue-shifted relative to the profiles measured by the Myers group in CCl_4 and the absorption spectra in both solvents, and large non-Condon couplings had to be included in the model in order to fit these profiles. They also obtained a large low-frequency reorganization energy of about 6200 cm^{-1} which, as discussed above, is probably best considered as representing some combination of true solvent contributions and those from unseen low-frequency intermolecular modes. These authors concluded, from the solvent dependence of the excitation profiles together with a variety of other observations, that the ground-state structure of the complex in CH_2Cl_2 is less symmetric than that in CCl_4, allowing mixing with and intensity borrowing from locally excited states of TCNE in the latter solvent. Indeed, much current thinking in the charge-transfer field calls into question the simple Mulliken picture which considers only two electronic states, the neutral ground state and the ion pair. Table 2 compares the final best-fit reorganization energies for the individual Raman-observable modes and for the solvent obtained by the Myers and McHale groups

Table 2. Mode-Specific Reorganization Energies for the Charge-Transfer Transition of HMB/TCNE in Two Solvents

in CCl_4[a]		in CH_2Cl_2[b]	
ω_g (cm^{-1})	λ_v (cm^{-1})	ω_g (cm^{-1})	λ_v (cm^{-1})
165	238	168	807
450	398		
542	73		
600	87		
968	94		
1292	233	1292	248
1386	63		
1437	38		
1551	601	1550	338
1570	66		
2222	215	2223	187
$E_0 = 13\ 910\ cm^{-1}$		$10\ 100\ cm^{-1}$	
$\lambda_s = 2550\ cm^{-1}$		$6200\ cm^{-1}$	

[a] Reference 96; from best simultaneous fit to absolute Raman profiles, absorption spectrum, and fluorescence spectrum. [b] Reference 95; from best simultaneous fit to absolute Raman profiles and absorption spectrum.

for HMB/TCNE in CCl_4 and in CH_2Cl_2, respectively.

Finally, very recently Pedron *et al.* reported resonance Raman excitation profiles of two solid salts containing π dimers of the radical cation of tetrathiafulvalene (TTF^+).[97] Spectra measured on resonance with the far-red (λ_{max} = 832 nm) charge-transfer absorption band of the dimer show strong resonance enhancement of three modes between 50 and 120 cm^{-1} that are assigned as intermolecular dimer modes, while the spectra excited at 530 nm, on resonance with locally excited transitions of TTF^+, show predominantly higher frequency modes localized on the TTF^+ monomers. The low-temperature charge-transfer Raman excitation profiles of the low-frequency modes were fit to a model that considers the TTF^+-localized modes to gain their activity through a standard Franck−Condon mechanism while the intermolecular modes, which modulate the distance and relative orientation of the monomers, become Raman-active through their effect on the electronic coupling between the two identical monomers.

V. Connections between Optical and Nonoptical Charge Transfer

The mode-specific vibrational reorganization energies in a charge-transfer process reveal both the changes in molecular geometry that accompany a large change in electron distribution and the energetics of the solvent's response to that altered charge distribution. While these quantities are certainly of interest in their own right for fundamental reasons, much of the interest in determining them arises from their appearance in the standard Golden Rule rate expression for nonradiative electron transfer. The usual sum-over-vibrational-states form of this expression implies that the reorganization parameters for all of the coupled modes must be known in order to calculate either the electron-transfer rate itself or its dependence on solvent or the chemical structure of the donor and/or acceptor.

More careful examination of the theoretical expressions, however, leads to the conclusion that generally the rate should *not* be very sensitive to the details of the individual modes' reorganization energies. The key is the close similarity between the expressions for the electron transfer rate and for ordinary optical absorption and emission band shapes. While the latter also depend in principle on the Franck−Condon factors (*i.e.* reorganization energies) for all of the coupled modes plus the solvent, in practice the spectra of ambient-temperature condensed-phase systems are usually far too diffuse for individual modes' contributions to be resolved. One can usually reproduce the absorption and fluorescence band shapes very well with models that include only one or a few vibrations and do not capture the full complexity of the Franck−Condon structure that underlies the spectrum. Indeed, the beauty of the resonance Raman technique is that is allows the experimentalist to dig out the mode-specific Franck−Condon information that is otherwise hidden. However, the formal expression for the vibrational part of the electron-transfer rate is identical to that for fluorescence (with a zero-frequency photon), implying that if an incomplete model is good enough to reproduce the fluorescence spectrum, it should also be adequate for the electron-transfer rate. All that is really needed is a model that fits the fluorescence extremely well on its low-energy side, such that the extrapolation to zero frequency will be good.

That being the case, there might seem to be little point to trying to decipher the vibrational structure that underlies diffuse charge-transfer absorption and fluorescence spectra if we are interested only in the rate for the nonradiative back transfer. For the most part this question simply has not been addressed in a critical way in the literature. Many disparate approaches to treating the vibrational reorganization, ranging from single-quantized-mode models to those that include the full multimode information obtained from resonance Raman intensities, seem to be able to account for experimental rate data.[98−101] The problem is that there are usually enough free parameters in the models, and/or a broad enough range of what is considered good agreement, that different models for the vibrational contribution cannot be distinguished. Only a few published studies have critically addressed the sensitivity of the calculated rates to the accuracy of the vibrational Franck−Condon information. Tominaga *et al.* showed that for the metal−metal charge-transfer reactions of the mixed-valence compound $(NH_3)_5Ru^{III}NCRu^{II}(CN)_5^-$, the calculated rates were affected little by grouping the eight vibrations observed in the resonance Raman spectra[74,102] into two "effective" modes, one high-frequency and one low-frequency.[100] Bixon *et al.* found that even a model system having nine significantly coupled modes with frequencies ranging from 150 to 2200 cm^{-1} could be very adequately reproduced by just one high-frequency mode as long as that mode's frequency and reorganization energy were optimized.[103] These results would not, of course, be expected to hold if the absorption and/or emission spectra exhibited resolved vibronic structure, but such structure is almost never observed in charge-transfer transitions (see Figures 8 and 9).

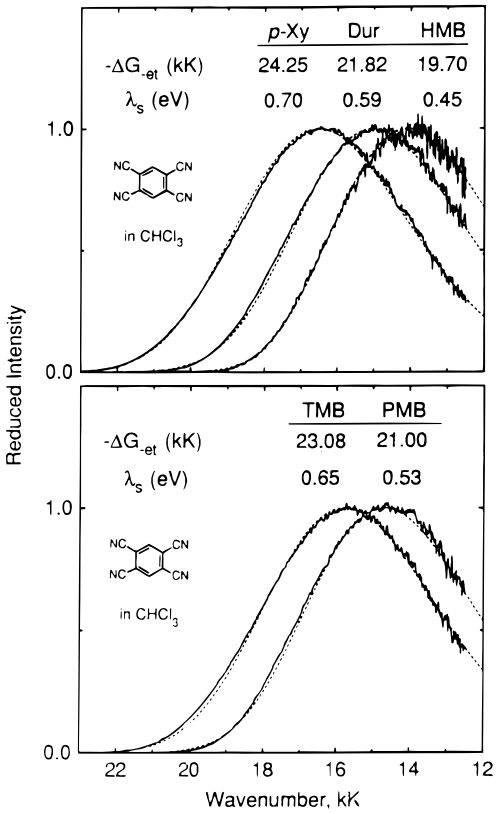

Figure 8. Reduced emission spectra (fluorescence intensity divided by frequency) for charge-transfer complexes of 1,2,4,5-tetracyanobenzene with various methyl-substituted benzene donors, in $CHCl_3$. Dashed curves are fits calculated using the indicated values for $-\Delta G_{-et}$ (the standard free energy difference between the radical ion pair and the neutral pair) and solvent reorganization energies, and a single high-frequency mode with $\omega = 1400\ cm^{-1}$ and $\lambda_v = 0.31$ eV. (Reproduced with permission from ref 101. Copyright 1993 Elsevier Science.)

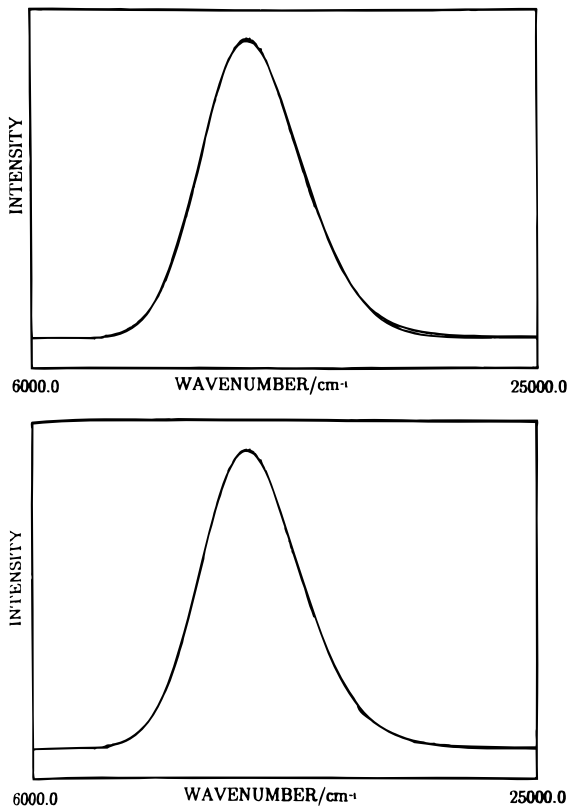

Figure 9. Observed and simulated absorption spectra of $(NH_3)_5Ru^{III}NCRu^{II}(CN)_5^-$ in D_2O, using eight modes obtained from a resonance Raman intensity analysis (top) and using just one mode (bottom). (Reproduced with permission from ref 100. Copyright 1993 American Institute of Physics.)

The one place where mode-specific vibrational reorganization energies really should be relevant is in rationalizing isotope effects on electron-transfer rates.[1,9,18,96,104−109] Isotopic substitution ought to be the closest thing to a pure Franck−Condon effect in that it presumably does not affect the electronic coupling and changes the energetics only through its differential influence on the zero-point energies, itself a type of Franck−Condon effect (if the neutral and ion-pair states had the same vibrational frequencies, there would be no isotope effect on ΔE_0). Many electron-transfer rates are indeed substantially affected by isotopic substitution of the reacting species and/or the solvent.[96,105,106,108,110−113] Surprisingly, with a few exceptions[112] these effects cannot be rationalized quantitatively or even qualitatively with the spectra (either absorption/fluorescence or resonance Raman), which usually show almost no effect of isotopic substitution. Reference 96 contains a more complete discussion of the isotope effect problem and points out analogies between electron transfer and other nonradiative electronic transitions in this regard.

VI. Conclusions and Prospects

The most *direct* way to determine the frequencies and reorganization energies of the high-frequency molecular vibrations coupled to electron-transfer processes is to measure vibrational spectra and crystal structures for both the reactants and the products.[114] However, this requires that both reactants and products be stable species, and the possibility that the solution and crystal structures may differ remains an important limitation. Theory can also provide guidance, but calculated geometries and vibrational frequencies for large open-shell ions in solution are still of questionable accuracy. Resonance Raman intensity analysis is appealing because it provides an "in situ" experimental probe of the geometry changes and reorganization energies that accompany electron-transfer processes occurring in complex molecular systems in a variety of environments. Resonance Raman-based techniques are, however, far from entirely general in that they can be applied only to systems in which an allowed radiative transition couples the initial and final states in the charge-transfer process. Furthermore, there are always far more parameters needed to characterize the charge-transfer transition than can be determined by fitting the data unless rather oversimplified models (*e.g.* harmonic modes with equal ground- and excited-state frequencies) are employed. It is probably unrealistic to expect spectral analysis alone to produce a truly complete picture of the geometry changes accompanying electron transfer in large molecules, but coupling increasingly powerful methods for electronic structure calculations with improved approaches to spectral modeling should allow increasingly precise conclusions to be drawn.

What is not so clear is the relevance of spectroscopically determined reorganization energies for predicting or rationalizing electron-transfer rates. Experimental results and simple theoretical considerations indicate that the complete set of frequencies and reorganization energies is not necessary, or at least not particularly helpful, for evaluating the FCWD in eqs 1 and 2. The inconsistency between spectroscopic and kinetic deuterium isotope effects for several systems suggests either that eq 1 is inadequate (most likely, that the assumed separability of electronic and nuclear contributions to the matrix element is incorrect) or that spectroscopic information is not enough to permit accurate evaluation of the FCWD. These are questions that must be resolved by experiment and theory working in concert. Time-resolved pump−probe infrared and Raman experiments, while technically difficult, hold great promise as methods that can directly observe the vibrations that accept the excess energy in return electron-transfer reactions.[115−117]

A fruitful direction for the future lies in combining the results of traditional frequency-domain resonance Raman spectroscopy with its all-time-domain analog (femtosecond resonant impulsive stimulated Raman scattering, or RISRS)[100,113,118−127] in order to capture the full range of vibrational frequencies coupled to the electron-transfer reaction.[128] The time-domain techniques are easiest to perform and most sensitive at the low-frequency end (below 100 cm^{-1}), which is precisely where frequency-domain Raman is most difficult due to interfering laser and Rayleigh scattering.[129] The combination of time- and frequency-domain spectroscopies has already been shown to be a powerful method for obtaining the complete spectral density of electronically nonresonant associated liquids such as water that have many low-frequency intermolecular vibrations.[130] This combination of techniques has also revealed apparent coupling of low-frequency solvent or intermolecular modes to electronic transitions of ions in polar solvents.[127] Charge-transfer transitions similarly involve a wide range of frequencies for the coupled vibrations ranging from high-frequency molecular modes to strongly overdamped solvent modes as well as, probably, vibrations that experience intermediate damping. The wide range of frequencies involved in the dynamics calls for the application of techniques spanning a wide range of time scales.

Acknowledgments

This work was supported by the NSF Science and Technology Center for Photoinduced Charge Transfer (CHE-9120001). A.M. is an NSF Presidential Young Investigator awardee and a Camille and Henry Dreyfus Teacher−Scholar. I thank Ian Gould, Alan Johnson, Shaul Mukamel, and Ralph Young for insightful discussions on the theory and practice of electron transfer, and Paul Barbara, Robin Clark, Joe Hupp, Glen Loppnow, Keitaro Yoshihara, and Jeff Zink for transmitting reprints or preprints of their work.

References

(1) Ulstrup, J.; Jortner, J. *J. Chem. Phys.* **1975**, *63*, 4358.
(2) Kestner, N. R.; Logan, J.; Jortner, J. *J. Phys. Chem.* **1974**, *78*, 2148.
(3) Jortner, J.; Bixon, M. *J. Chem. Phys.* **1988**, *88*, 167.
(4) Marcus, R. A. *J. Chem. Phys.* **1984**, *81*, 4494.
(5) Marcus, R. A. *J. Chem. Phys.* **1965**, *43*, 1261.
(6) Marcus, R. A.; Sutin, N. *Comments Inorg. Chem.* **1986**, *5*, 119.
(7) Marcus, R. A. *J. Phys. Chem.* **1989**, *93*, 3078.
(8) Marcus, R. A. *Annu. Rev. Phys. Chem.* **1964**, *15*, 155.
(9) Buhks, E.; Bixon, M.; Jortner, J.; Navon, G. *J. Phys. Chem.* **1981**, *85*, 3759.
(10) Siders, P.; Marcus, R. A. *J. Am. Chem. Soc.* **1981**, *103*, 741.
(11) Siders, P.; Marcus, R. A. *J. Am. Chem. Soc.* **1981**, *103*, 748.
(12) Siebrand, W. *J. Chem. Phys.* **1967**, *46*, 440.
(13) Siebrand, W.; Williams, D. F. *J. Chem. Phys.* **1968**, *49*, 1860.
(14) Mortensen, O. S.; Siebrand, W.; Tarr, A. W. *Chem. Phys.* **1988**, *125*, 231.
(15) Englman, R.; Jortner, J. *Mol. Phys.* **1970**, *18*, 145.
(16) Freed, K. F.; Jortner, J. *J. Chem. Phys.* **1970**, *52*, 6272.
(17) Mukamel, S.; Yan, Y. J. *Acc. Chem. Res.* **1989**, *22*, 301.
(18) Jortner, J. *J. Chem. Phys.* **1976**, *64*, 4860.
(19) Myers, A. B. *Chem. Phys.* **1994**, *180*, 215.
(20) Yan, Y. J.; Mukamel, S. *J. Chem. Phys.* **1991**, *94*, 179.
(21) Myers, A. B. In *Laser Techniques in Chemistry*; Myers, A. B., Rizzo, T. R., Ed.; Wiley: New York, 1995; p 325.
(22) Johnson, A. E.; Myers, A. B. *J. Phys. Chem.*, in press.
(23) Kramers, H. A.; Heisenberg, W. *Z. Phys.* **1925**, *31*, 681.
(24) Dirac, P. A. M. *Proc. R. Soc. (London)* **1927**, *114*, 710.
(25) Tang, J.; Albrecht, A. C. In *Raman Spectroscopy*; Szymanski, H. A., Ed.; Plenum: New York, 1970; Vol. 2, p 33.
(26) Lee, S.-Y.; Heller, E. J. *J. Chem. Phys.* **1979**, *71*, 4777.
(27) Heller, E. J.; Sundberg, R. L.; Tannor, D. *J. Phys. Chem.* **1982**, *86*, 1822.
(28) Myers, A. B. *J. Opt. Soc. Am. B* **1990**, *7*, 1665.
(29) Myers, A. B.; Mathies, R. A. In *Biological Applications of Raman Spectroscopy*; Spiro, T. G., Ed.; Wiley: New York, 1987; Vol. 2, p 1.
(30) Zink, J. I.; Shin, K.-S. K. *Adv. Photochem.* **1991**, *16*, 119.
(31) Harris, R. A.; Mathies, R.; Myers, A. *Chem. Phys. Lett.* **1983**, *94*, 327.
(32) Phillips, D. L.; Myers, A. B. *J. Chem. Phys.* **1991**, *95*, 226.
(33) Markel, F.; Myers, A. B. *J. Chem. Phys.* **1993**, *98*, 21.
(34) Galica, G. E.; Johnson, B. R.; Kinsey, J. L.; Hale, M. O. *J. Phys. Chem.* **1991**, *95*, 7994.
(35) Heller, E. J. *Acc. Chem. Res.* **1981**, *14*, 368.
(36) Tonks, D. L.; Page, J. B. *Chem. Phys. Lett.* **1979**, *66*, 449.
(37) Page, J. B.; Tonks, D. L. *J. Chem. Phys.* **1981**, *75*, 5694.
(38) Tonks, D. L.; Page, J. B. *J. Chem. Phys.* **1982**, *76*, 5820.
(39) Chan, C. K.; Page, J. B. *J. Chem. Phys.* **1983**, *79*, 5234.
(40) Lu, H. M.; Page, J. B. *J. Chem. Phys.* **1988**, *88*, 3508.
(41) Lu, H. M.; Page, J. B. *J. Chem. Phys.* **1990**, *92*, 7038.
(42) Stallard, B. R.; Champion, P. M.; Callis, P. R.; Albrecht, A. C. *J. Chem. Phys.* **1983**, *78*, 712.
(43) Stallard, B. R.; Callis, P. R.; Champion, P. M.; Albrecht, A. C. *J. Chem. Phys.* **1984**, *80*, 70.
(44) Gu, Y.; Champion, P. M. *Chem. Phys. Lett.* **1990**, *171*, 254.
(45) Patapoff, T. W.; Turpin, P.-Y.; Peticolas, W. L. *J. Phys. Chem.* **1986**, *90*, 2347.
(46) Cable, J. R.; Albrecht, A. C. *J. Chem. Phys.* **1986**, *84*, 4745.
(47) Champion, P. M.; Albrecht, A. C. *Annu. Rev. Phys. Chem.* **1982**, *33*, 353.
(48) Albrecht, A. C.; Clark, R. J. H.; Oprescu, D.; Owens, S. J. R.; Svendsen, C. *J. Chem. Phys.* **1994**, *101*, 1890.
(49) Svendsen, C.; Mortensen, O. S.; Clark, R. J. H. *Chem. Phys.* **1994**, *187*, 349.
(50) Cable, J. R.; Albrecht, A. C. *J. Chem. Phys.* **1986**, *84*, 1969.
(51) Sue, J.; Yan, Y. J.; Mukamel, S. *J. Chem. Phys.* **1986**, *85*, 462.
(52) Yan, Y. J.; Mukamel, S. *J. Chem. Phys.* **1987**, *86*, 6085.
(53) Lee, D.; Albrecht, A. C. *Adv. Infrared Raman Spectrosc.* **1985**, *12*, 179.
(54) Ziegler, L. D. *Acc. Chem. Res.* **1994**, *27*, 1.
(55) Fan, R.; Kalbfleisch, T.; Ziegler, L. D. *J. Chem. Phys.* **1996**, *104*, 3886.
(56) Reilly, P. D.; Skinner, J. L. *J. Chem. Phys.* **1994**, *101*, 959.
(57) Mukamel, S.; Yan, Y. J. In *Recent trends in Raman spectroscopy*; Banerjee, S. B., Jha, S. S., Ed.; World Scientific: Singapore, 1989; p 160.
(58) Mukamel, S. *J. Chem. Phys.* **1985**, *82*, 5398.
(59) Takagahara, T.; Hanamura, E.; Kubo, R. *J. Phys. Soc. Jpn.* **1977**, *43*, 802.
(60) Watanabe, J.; Kinoshita, S.; Kushida, T. *Chem. Phys. Lett.* **1986**, *126*, 197.
(61) Nibbering, E. T. J.; Duppen, K.; Wiersma, D. A. *J. Chem. Phys.* **1990**, *93*, 5477.
(62) Gu, Y.; Widom, A.; Champion, P. M. *J. Chem. Phys.* **1994**, *100*, 2547.
(63) Li, B.; Johnson, A. E.; Mukamel, S.; Myers, A. B. *J. Am. Chem. Soc* **1994**, *116*, 11039.

(64) Mukamel, S. *Principles of nonlinear optical spectroscopy*; Oxford University Press: New York, 1995.
(65) Tanimura, Y.; Mukamel, S. *J. Opt. Soc. Am. B* **1993**, *10*, 2263.
(66) Yan, Y. J.; Mukamel, S. *Phys. Rev. A* **1990**, *41*, 6485.
(67) Bosma, W. B.; Yan, Y. J.; Mukamel, S. *Phys. Rev. A* **1990**, *42*, 6920.
(68) Wright, P. G.; Stein, P.; Burke, J. M.; Spiro, T. G. *J. Am. Chem. Soc.* **1979**, *101*, 3531.
(69) Warshel, A. *Annu. Rev. Biophys. Bioeng.* **1977**, *6*, 273.
(70) Blazej, D. C.; Peticolas, W. L. *Proc. Natl. Acad. Sci. U.S.A.* **1977**, *74*, 2639.
(71) Peticolas, W. L.; Strommen, D. P.; Lakshminarayanan, V. *J. Chem. Phys.* **1980**, *73*, 4185.
(72) Yang, Y.-Y.; Zink, J. I. *J. Am. Chem. Soc.* **1984**, *106*, 1500.
(73) Doorn, S. K.; Hupp, J. T. *J. Am. Chem. Soc.* **1989**, *111*, 4704.
(74) Doorn, S. K.; Hupp, J. T. *J. Am. Chem. Soc.* **1989**, *111*, 1142.
(75) Berger, R. M.; McMillin, D. R. *Inorg. Chim. Acta* **1990**, *177*, 65.
(76) Maruszewski, K.; Bajdor, K.; Strommen, D. P.; Kincaid, J. R. *J. Phys. Chem.* **1995**, *99*, 6286.
(77) Fraga, E.; Webb, M. A.; Loppnow, G. R. *J. Phys. Chem.* **1996**, *100*, 3278.
(78) Markel, F.; Ferris, N. S.; Gould, I. R.; Myers, A. B. *J. Am. Chem. Soc.* **1992**, *114*, 6208.
(79) Wootton, J. L.; Zink, J. I. *J. Phys. Chem.* **1995**, *99*, 7251.
(80) Hush, N. S. *Prog. Inorg. Chem.* **1967**, *8*, 391.
(81) Hush, N. S. *Coord. Chem. Rev.* **1985**, *64*, 135.
(82) Doorn, S. K.; Blackbourn, R. L.; Johnson, C. S.; Hupp, J. T. *Electrochim. Acta* **1991**, *36*, 1775.
(83) Clark, R. J. H.; Dines, T. J. *Chem. Phys. Lett.* **1991**, *185*, 490.
(84) Doorn, S. K.; Hupp, J. T.; Porterfield, D. R.; Campion, A.; Chase, D. B. *J. Am. Chem. Soc.* **1990**, *112*, 4999.
(85) Lu, H.; Petrov, V.; Hupp, J. T. *Chem. Phys. Lett.* **1995**, *235*, 521.
(86) Petrov, V.; Hupp, J. T.; Mottley, C.; Mann, L. C. *J. Am. Chem. Soc.* **1994**, *116*, 2171.
(87) Creutz, C. *Prog. Inorg. Chem.* **1983**, *30*, 1.
(88) Blackbourn, R. L.; Johnson, C. S.; Hupp, J. T. *J. Am. Chem. Soc.* **1991**, *113*, 1060.
(89) Blackbourn, R. L.; Johnson, C. S.; Hupp, J. T.; Bryant, M. A.; Sobocinski, R. L.; Pemberton, J. E. *J. Phys. Chem.* **1991**, *95*, 10535.
(90) Michaelian, K. H.; Rieckhoff, K. E.; Voigt, E.-M. *Proc. Nat. Acad. Sci. U.S.A.* **1975**, *72*, 4196.
(91) Smith, M. L.; McHale, J. L. *J. Phys. Chem.* **1985**, *89*, 4002.
(92) McHale, J. L.; Merriam, M. J. *J. Phys. Chem.* **1989**, *93*, 526.
(93) Britt, B. M.; Lueck, H. B.; McHale, J. L. *Chem. Phys. Lett.* **1992**, *190*, 528.
(94) Kulinowski, K.; Gould, I. R.; Myers, A. B. *J. Phys. Chem.* **1995**, *99*, 9017.
(95) Britt, B. M.; McHale, J. L.; Friedrich, D. M. *J. Phys. Chem.* **1995**, *99*, 6347.
(96) Kulinowski, K.; Gould, I. R.; Ferris, N. S.; Myers, A. B. *J. Phys. Chem.* **1995**, *99*, 17715.
(97) Pedron, D.; Speghini, A.; Mulloni, V.; Bozio, R. *J. Chem. Phys.* **1995**, *103*, 2795.
(98) Katz, N. E.; Mecklenburg, S. L.; Graff, D. K.; Chen, P.; Meyer, T. J. *J. Phys. Chem.* **1994**, *98*, 8959.
(99) Walker, G. C.; Åkesson, E.; Johnson, A. E.; Levinger, N. E.; Barbara, P. F. *J. Phys. Chem.* **1992**, *96*, 3728.
(100) Tominaga, K.; Kliner, D. A. V.; Johnson, A. E.; Levinger, N. E.; Barbara, P. F. *J. Chem. Phys.* **1993**, *98*, 1228.
(101) Gould, I. R.; Noukakis, D.; Gomez-Jahn, L.; Young, R. H.; Goodman, J. L.; Farid, S. *Chem. Phys.* **1993**, *176*, 439.
(102) Walker, G. C.; Barbara, P. F.; Doorn, S. K.; Dong, Y.; Hupp, J. T. *J. Phys. Chem.* **1991**, *95*, 5712.
(103) Bixon, M.; Jortner, J.; Cortes, J.; Heitele, H.; Michel-Beyerle, M. E. *J. Phys. Chem.* **1994**, *98*, 7289.
(104) Bader, J. S.; Kuharski, R. A.; Chandler, D. *J. Chem. Phys.* **1990**, *93*, 230.
(105) Doolen, R.; Simon, J. D.; Baldridge, K. K. *J. Phys. Chem.* **1995**, *99*, 13938.
(106) Gould, I. R.; Farid, S. *J. Am. Chem. Soc.* **1988**, *110*, 7883.
(107) Yoshihara, K.; Tominaga, K.; Nagasawa, Y. *Bull. Chem. Soc. Jpn.* **1995**, *68*, 696.
(108) Nagasawa, Y.; Yartsev, A. P.; Tominaga, K.; Yoshihara, K. In *Ultrafast Phenomena IX*; Barbara, P. F., Knox, W. H., Mourou, G. A., Zewail, A. H., Ed.; Springer-Verlag: Berlin Heidelberg, 1994; p 84.
(109) Buhks, E.; Bixon, M.; Jortner, J. *J. Phys. Chem.* **1981**, *85*, 3763.
(110) Dresner, J.; Prochorow, J.; Sobolewski, A. *Chem. Phys. Lett.* **1978**, *54*, 292.
(111) Okajima, S.; Lim, B. T.; Lim, E. C. *J. Chem. Phys.* **1980**, *73*, 3512.
(112) Khoshtariya, D. E.; Meusinger, R.; Billing, R. *J. Phys. Chem.* **1995**, *99*, 3592.
(113) Reid, P. J.; Silva, C.; Barbara, P. F.; Karki, L.; Hupp, J. T. *J. Phys. Chem.* **1995**, *99*, 2609.
(114) Fischer, S. F.; Van Duyne, R. P. *Chem. Phys.* **1977**, *26*, 9.
(115) Vauthey, E.; Phillips, D.; Parker, A. W. *J. Phys. Chem.* **1992**, *96*, 7356.
(116) Doorn, S. K.; Stoutland, P. O.; Dyer, R. B.; Woodruff, W. H. *J. Am. Chem. Soc.* **1992**, *114*, 3133.
(117) Doorn, S. K.; Dyer, R. B.; Stoutland, P. O.; Woodruff, W. H. *J. Am. Chem. Soc.* **1993**, *115*, 6398.
(118) Vöhringer, P.; Scherer, N. F. *J. Phys. Chem.* **1995**, *99*, 2684.
(119) Dexheimer, S. L.; Wang, Q.; Peteanu, L. A.; Pollard, W. T.; Mathies, R. A.; Shank, C. V. *Chem. Phys. Lett.* **1992**, *188*, 61.
(120) Pollard, W. T.; Dexheimer, S. L.; Wang, Q.; Peteanu, L. A.; Shank, C. V.; Mathies, R. A. *J. Phys. Chem.* **1992**, *96*, 6147.
(121) Banin, U.; Ruhman, S. *J. Chem. Phys.* **1993**, *98*, 4391.
(122) Zhu, L.; Sage, J. T.; Champion, P. M. *Science* **1994**, *266*, 629.
(123) Chachisvilis, M.; Fidder, H.; Pullerits, T.; Sundström, V. *J. Raman Spectrosc.* **1995**, *26*, 513.
(124) Scherer, N. F.; Ziegler, L. D.; Fleming, G. R. *J. Chem. Phys.* **1992**, *96*, 5544.
(125) Zadoyan, R.; Li, Z.; Martens, C. C.; Apkarian, V. A. *J. Chem. Phys.* **1994**, *101*, 6648.
(126) Wynne, K.; Galli, C.; Hochstrasser, R. M. *J. Chem. Phys.* **1994**, *100*, 4797.
(127) Johnson, A. E.; Myers, A. B. *J. Chem. Phys.*, in press.
(128) Arnett, D. C.; Vöhringer, P.; Scherer, N. F. *J. Am. Chem. Soc.* **1995**, *117*, 12262.
(129) Dhar, L.; Rogers, J. A.; Nelson, K. A. *Chem. Rev.* **1994**, *94*, 157.
(130) Castner, E. W., Jr.; Chang, Y. J.; Chu, Y. C.; Walrafen, G. E. *J. Chem. Phys.* **1995**, *102*, 653.
(131) Kulinowski, K. Ph.D. Thesis, University of Rochester, 1995.

CR950249C